J. Fluid Mech. (1985), *vol.* 153, *pp.* 243–258
Printed in Great Britain

A numerical and experimental study of anomalous modes in the Taylor experiment

By K. A. CLIFFE
Theoretical Physics Division, AERE Harwell, Didcot, Oxon OX11 0RA

AND T. MULLIN
Clarendon Laboratory, Parks Road, Oxford OX1 3PU

(Received 2 August 1984)

Anomalous modes are flows in the Taylor experiment that exist only for sufficiently high Reynolds number R and are always distinct from the primary flow produced by gradually increasing R from small values. They are distinguished from all other secondary modes by having a direction of spiralling of one or both of the end cells such that outward flow is found along the stationary endwall. In this paper we present new observations of these flows and compare them with numerical solutions of the Navier–Stokes equations. A numerical technique for calculating anomalous modes is described and stability curves for 2-, 3-, and 4-cell flows are presented. Streamline plots of the numerical solutions are compared with photographs of the observed flows. The agreement between the calculations and experiments is good. The calculations also confirm certain theoretical predictions made by Benjamin (1978), Benjamin & Mullin (1981) and Hall (1982).

1. Introduction

The aim of the present numerical and experimental investigation is to extend our knowledge of the role of finite-length effects in rotary Taylor–Couette flow. To this end, we have studied a class of steady flows which exist at sufficiently high values of the Reynolds number R. They have been called 'anomalous modes' by Benjamin (1978) and have been studied in detail for a range of parameters by Benjamin (1978) and Benjamin & Mullin (1981).

The flows under consideration are generated in an apparatus with a rotating inner cylinder and a concentric stationary outer cylinder with stationary endwalls. Under these conditions, the cellular flow which is evolved by continuous increase in speed of the inner cylinder from rest consists of an even number of cells. The direction of spiralling of the end cells is such that the flow is inwards on the endwall, which is consistent with the fact that the centrifugal force is reduced owing to the no-slip condition applying to the azimuthal component of velocity. A flow formed in this way is defined to be the primary mode and it is uniquely prescribed for a given length of the apparatus. The mutation of the primary flow, as the length of the flow domain is changed, is now well understood, e.g. see Mullin (1982) and Cliffe (1984) for complementary experimental and numerical studies.

In addition to the above flows, other flows with direction of spiralling of the end cells in the opposite sense were first discovered by Benjamin (1978). He found that either one or both end cells rotated such that outward flow is found along the fixed endwall, so that one may observe an array of cells of either odd or even number. These

flows are all disconnected from the primary flow except for the special case of a single cell as found by Benjamin & Mullin (1981) and subsequently studied numerically by Cliffe (1983). Therefore, the anomalous modes cannot survive below a critical value of R which depends upon the aspect ratio. It is an unusual fact that these modes have apparently gone undetected by other researchers in this field but this may be due to the fact that their domain of existence is far removed from that of the normal steady Taylor cells.

Benjamin & Mullin (1981) also gave a theoretical account of the anomalous modes based on a model, for boundary effects in Taylor–Couette flow, which was proposed by Schaeffer (1980). Schaeffer's model has also been studied in a quantitative manner by Hall (1980, 1982). We shall review the Schaeffer model and its application to the anomalous modes in §2. An interesting feature of the anomalous modes is that away from the ends of the annulus the flow resembles a normal mode in that the cells are approximately periodically spaced and of the same size as their normal counterparts. However, the critical Reynolds number above which they are possible is at least twice that for onset of Taylor vortices according to the periodic- or infinite-cylinder model. The stability of the entire flow is governed by the stability of the end cell or cells, emphasizing the fact that these flows are not small perturbations of the flows originating in the periodic model. Consequently we believe that numerical techniques are the only available means of obtaining quantitative comparison between theory and experiment.

Although we only consider relatively short cylinders here, complementary experimental studies by Benjamin & Mullin (1982) and Lorenzen & Mullin (1984) indicate that the properties of anomalous modes are similar over a wide range of cylinder lengths. Lorenzen & Mullin (1984) studied the stability of the anomalous 40-cell mode and found results very similar to those presented here. We should further note that similar even- and odd-cell anomalous modes have been observed by Mullin & Lorenzen (1984) in their experiment on the flow in the gap between a square-sectioned stationary outer cylinder and a rotating circular cylinder. In addition, an even-cell anomalous mode has been observed in Taylor–Couette flow with asymmetric end boundaries by Mullin, Cliffe & Benjamin (1984). Also, for the buoyancy-driven flow in a tilted cavity Cliffe & Winters (1984) calculated convective flows which are analogous to the anomalous modes of the Taylor experiment.

The purpose of the present paper is to present numerical calculations of anomalous modes which will be compared with new experimental observations. We shall compare computed and measured stability curves and also computed streamline plots with photographs of the anomalous modes. The numerical methods are similar to those used to investigate 2-cell and single-cell flows (Cliffe 1983) and the primary flow exchange process (Cliffe 1984). Continuation methods and methods for bifurcation problems are applied to a finite-element discretization of the Navier–Stokes equations. Since the anomalous modes are not continuously connected to the primary flow their generation is not entirely straightforward. We shall present a technique by which any anomalous mode may be systematically calculated. This will be described in detail in §3 after the basic numerical methods have been summarized.

The experimental procedure we used is similar to that of Benjamin & Mullin (1981) and it will be described in §4. In §5 we shall present our results including a comparison between the calculations and experimental data. Finally, in §6 we shall draw some conclusions and emphasize the important and necessary role the anomalous modes play in Taylor–Couette flow.

flows are all disconnected from the primary flow except for the special case of a single cell as found by Benjamin & Mullin (1981) and subsequently studied numerically by Cliffe (1983). Therefore, the anomalous modes cannot survive below a critical value of R which depends upon the aspect ratio. It is an unusual fact that these modes have apparently gone undetected by other researchers in this field but this may be due to the fact that their domain of existence is far removed from that of the normal steady Taylor cells.

Benjamin & Mullin (1981) also gave a theoretical account of the anomalous modes based on a model, for boundary effects in Taylor–Couette flow, which was proposed by Schaeffer (1980). Schaeffer's model has also been studied in a quantitative manner by Hall (1980, 1982). We shall review the Schaeffer model and its application to the anomalous modes in §2. An interesting feature of the anomalous modes is that away from the ends of the annulus the flow resembles a normal mode in that the cells are approximately periodically spaced and of the same size as their normal counterparts. However, the critical Reynolds number above which they are possible is at least twice that for onset of Taylor vortices according to the periodic- or infinite-cylinder model. The stability of the entire flow is governed by the stability of the end cell or cells, emphasizing the fact that these flows are not small perturbations of the flows originating in the periodic model. Consequently we believe that numerical techniques are the only available means of obtaining quantitative comparison between theory and experiment.

Although we only consider relatively short cylinders here, complementary experimental studies by Benjamin & Mullin (1982) and Lorenzen & Mullin (1984) indicate that the properties of anomalous modes are similar over a wide range of cylinder lengths. Lorenzen & Mullin (1984) studied the stability of the anomalous 40-cell mode and found results very similar to those presented here. We should further note that similar even- and odd-cell anomalous modes have been observed by Mullin & Lorenzen (1984) in their experiment on the flow in the gap between a square-sectioned stationary outer cylinder and a rotating circular cylinder. In addition, an even-cell anomalous mode has been observed in Taylor–Couette flow with asymmetric end boundaries by Mullin, Cliffe & Benjamin (1984). Also, for the buoyancy-driven flow in a tilted cavity Cliffe & Winters (1984) calculated convective flows which are analogous to the anomalous modes of the Taylor experiment.

The purpose of the present paper is to present numerical calculations of anomalous modes which will be compared with new experimental observations. We shall compare computed and measured stability curves and also computed streamline plots with photographs of the anomalous modes. The numerical methods are similar to those used to investigate 2-cell and single-cell flows (Cliffe 1983) and the primary flow exchange process (Cliffe 1984). Continuation methods and methods for bifurcation problems are applied to a finite-element discretization of the Navier–Stokes equations. Since the anomalous modes are not continuously connected to the primary flow their generation is not entirely straightforward. We shall present a technique by which any anomalous mode may be systematically calculated. This will be described in detail in §3 after the basic numerical methods have been summarized.

The experimental procedure we used is similar to that of Benjamin & Mullin (1981) and it will be described in §4. In §5 we shall present our results including a comparison between the calculations and experimental data. Finally, in §6 we shall draw some conclusions and emphasize the important and necessary role the anomalous modes play in Taylor–Couette flow.

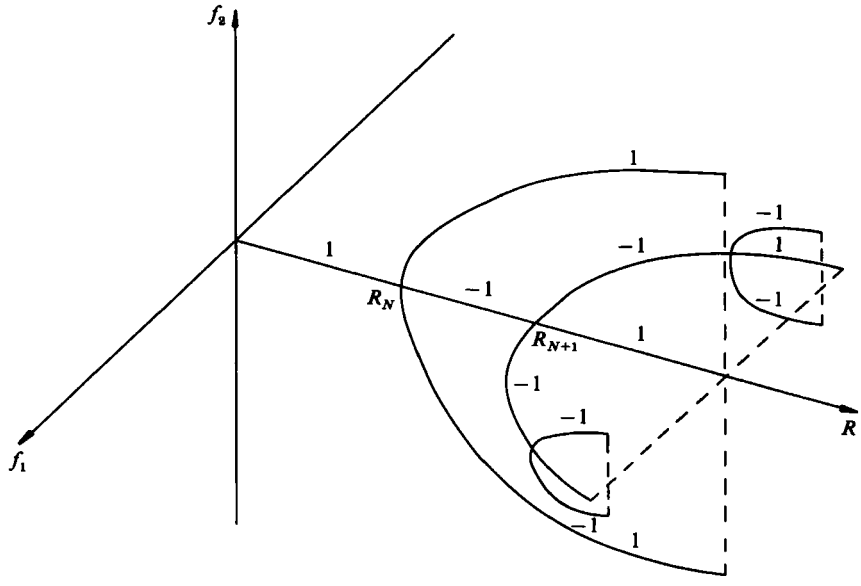

FIGURE 1. Representation of the complete solution set for successive supercritical bifurcations.

2. Schaeffer's model

A detailed discussion of the application of Schaeffer's model to the problem of anomalous modes in the Taylor experiment has already been given by Benjamin & Mullin (1981) and Hall (1982). We shall briefly review this work and refer the reader to Schaeffer's (1980) original paper and the above references for details. Schaeffer's idea was to introduce a parameter $\tau \in [0, 1]$ into the problem in such a way that when $\tau = 0$ one has the well-known periodic problem and when $\tau = 1$ one has the realistic case of stationary ends. He did this by applying the following boundary conditions to the region $\{(r, z) \mid r_1 \leqslant r \leqslant r_2,\ -\frac{1}{2}l \leqslant z \leqslant \frac{1}{2}l\}$,

$$\left.\begin{aligned} u_z &= 0, \\ (1-\tau)\frac{\partial u_r}{\partial z} \pm \tau u_r &= 0, \\ (1-\tau)\frac{\partial u_\phi}{\partial z} \pm \tau\{u_\phi - F(r)\} &= 0, \end{aligned}\right\} \quad \text{for } z = \pm\tfrac{1}{2}l, \quad r_1 \leqslant r \leqslant r_2, \tag{2.1}$$

where $F(r)$ is a smooth function satisfying $F(r_1) = 1$ and $F(r) = 0$ for $r \geqslant r_1 + \delta$, with $0 < \delta \ll r_2 - r_1$. This function is introduced so that the solutions of the realistic problem have a finite rate of dissipation of energy (see Benjamin & Mullin 1981 pp. 224, 225). The case $\tau = 0$ corresponds to the periodic problem for which a great deal of analytical information is available. Schaeffer analysed this problem close to the point where two different modes become unstable at the same value of Reynolds number, and allowed for the effects of non-zero τ using the methods of singularity theory. The relevant case here is where the two modes have N and $N+1$ cells respectively. Schaeffer only treated the interaction between modes having an even number of cells; the present treatment is due to Benjamin & Mullin (1981). The solution set for this case is illustrated in figure 1. The N-cell solution bifurcates from the trivial (Couette flow) solution at R_N and the $(N+1)$-cell solution bifurcates at

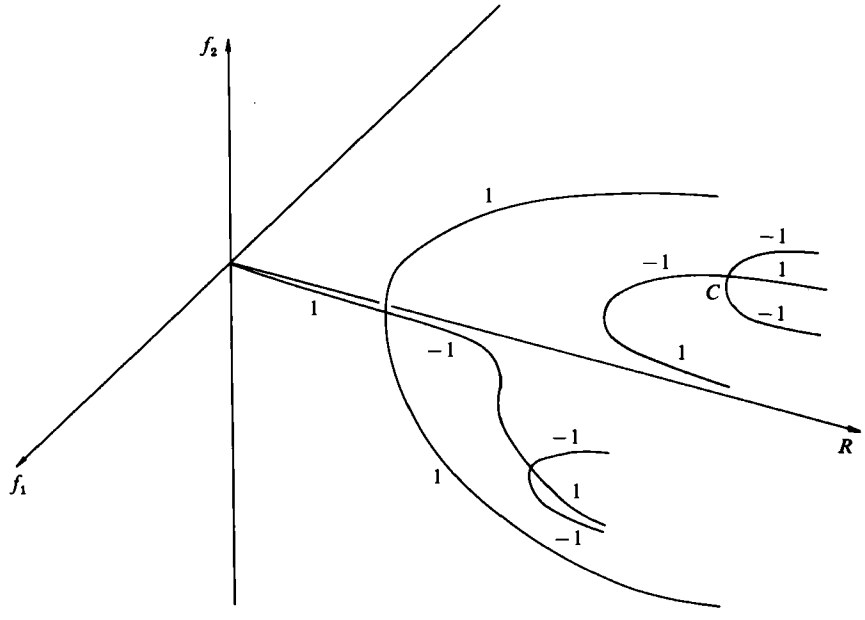

FIGURE 2. Perturbed bifurcation diagram illustrating the anomalous modes (cf. figure 1).

R_{N+1}. The $(N+1)$-cell branch suffers secondary bifurcations which are associated with the multiple eigenvalue that occurs when l is chosen to make R_N and R_{N+1} equal (Bauer, Keller & Reiss 1975; Shearer 1980). The $(N+1)$-cell branch is stable for R greater than the value at which the secondary bifurcation occurs. If N is odd then f_1 is a measure of the symmetric component of the solution and f_2 measures the antisymmetric component. The effect of non-zero τ is to split the bifurcation at R_{N+1}, but, because of the symmetry, the other bifurcations are not split. The situation for small τ is shown in figure 2. It is now clear where the even, $(N+1)$-cell anomalous mode comes from. The branch above the bifurcation at C is a perturbation of the $(N+1)$-cell flow in the periodic problem with flow outwards near the planes $z = \pm\frac{1}{2}l$. Note that in the periodic problem the two $(N+1)$-cell bifurcating branches have, alternatively, flow inwards and outwards near the ends. The branch with flow inwards becomes the primary branch as τ tends to one. Figure 2 also illustrates the possibility that the anomalous modes with an even number of cells may lose stability, not at a limit point, but at a supercritical symmetry-breaking bifurcation such as point C. The Leray–Schauder indices are indicated on this diagram and it is clear that, when the Reynolds number is reduced below that corresponding to C, all the nearby solutions have index -1 and are therefore unstable. We shall return to this point in §5.

The anomalous mode with N-cells bifurcates from the primary branch for small values of τ. However, Benjamin & Mullin (1981) argued that, except for the single-cell flows at very small aspect ratio, the anomalous modes with an odd number of cells would decouple from the primary branch via the process shown in figure 3; the quantitative study by Hall (1982) supports this conclusion. The bifurcation at A becomes subcritical and eventually coalesces with the secondary bifurcation at B to produce a pair of anomalous modes with an odd number of cells.

We conclude this section by emphasizing that, in the context of Schaeffer's model,

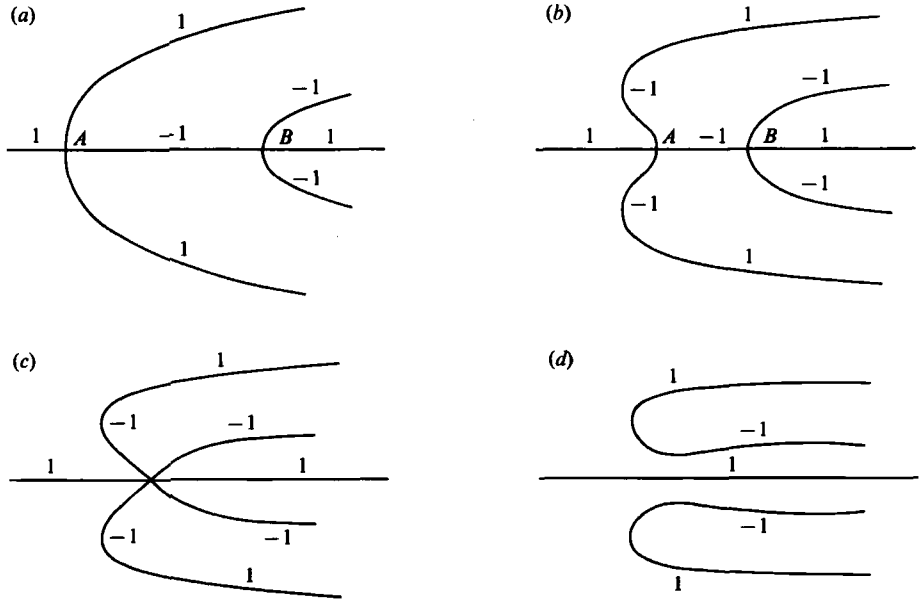

FIGURE 3. Changes in the bifurcation diagram for the anomalous modes having an odd number of cells (excluding the case with 1-cell) as the parameter τ increases from 0 to 1.

the anomalous modes are far from surprising; indeed they are to be expected. What is surprising is that they were apparently undetected until Benjamin's experiments in the seventies.

3. Numerical methods

In this section we shall briefly summarize the numerical methods we have used. They are similar to those in Cliffe (1983, 1984) and Cliffe & Winters (1984). Let r_1 and r_2 be the radii of the inner and outer cylinder respectively and let l be their length. Let Ω be the angular speed of the inner cylinder, the outer cylinder being taken to be stationary. In cylindrical polar coordinates (r^*, ϕ, z^*) with origin midway between the ends of the annulus and velocity $U^* \equiv (u_r^*, u_\phi^*, u_z^*)$, the equations for steady axisymmetric flow of a viscous fluid are:

$$R\left(\Gamma u_r \frac{\partial u_r}{\partial r} + u_z \frac{\partial u_r}{\partial z} - \frac{\Gamma u_\phi^2}{r+\beta}\right) + \Gamma \frac{\partial p}{\partial r} - \frac{\Gamma}{r+\beta}\frac{\partial}{\partial r} 2(r+\beta)\frac{\partial u_r}{\partial r} - \frac{\partial}{\partial z}\left(\frac{1}{\Gamma}\frac{\partial u_r}{\partial z} + \frac{\partial u_z}{\partial r}\right) + \frac{2\Gamma u_r}{(r+\beta)^2} = 0, \quad (3.1)$$

$$R\left(\Gamma u_r \frac{\partial u_\phi}{\partial r} + u_z \frac{\partial u_\phi}{\partial z} + \Gamma \frac{u_r u_\phi}{r+\beta}\right) - \frac{\Gamma}{r+\beta}\frac{\partial}{\partial r}(r+\beta)\frac{\partial u_\phi}{\partial r} - \frac{1}{\Gamma}\frac{\partial^2 u_\phi}{\partial z^2} + \frac{\Gamma u_\phi}{(r+\beta)^2} = 0, \quad (3.2)$$

$$R\left(\Gamma u_r \frac{\partial u_z}{\partial r} + u_z \frac{\partial u_z}{\partial z}\right) + \frac{\partial p}{\partial z} - \frac{1}{r+\beta}\frac{\partial}{\partial r}(r+\beta)\left(\Gamma \frac{\partial u_z}{\partial r} + \frac{\partial u_r}{\partial z}\right) - \frac{2}{\Gamma}\frac{\partial^2 u_z}{\partial z^2} = 0, \quad (3.3)$$

$$\frac{\Gamma}{r+\beta}\frac{\partial}{\partial r}(r+\beta)u_r + \frac{\partial u_z}{\partial z} = 0. \quad (3.4)$$

In the above equations r, z, U and p are given by

$$r = \frac{r^*}{d} - \beta, \quad z = \frac{z^*}{l}, \quad U = \frac{U^*}{r_1 \Omega}, \quad p = \frac{dp^*}{\mu r_1 \Omega},$$

where $d = r_2 - r_1$, $\beta = r_1/d = \eta/(1-\eta)$ and η is the radius ratio. The aspect ratio $\Gamma = l/d$ and the Reynolds number $R = \rho r_1 \Omega d/\mu$, where ρ and μ are the fluid density and viscosity respectively.

Equations (3.1)–(3.4) hold in the region

$$D = \{(r, z) \,|\, 0 \leqslant r \leqslant 1, \; -0.5 \leqslant z \leqslant 0.5\}. \tag{3.5}$$

The boundary conditions are that u_r and u_z are zero on the inner and outer cylinder, u_ϕ is 0 on the outer cylinder and 1 on the inner cylinder and we apply Schaeffer's conditions (2.1) on the ends of the annulus.

Equations (3.1)–(3.4) are discretized by the finite-element method. Details of this method are given in Cliffe (1983) and Cliffe & Spence (1984). We mention that we used nine-node quadrilateral elements; on each element the components of velocity are approximated by biquadratic polynomials and the pressure is approximated by piecewise linear functions which are not, in general, continuous across element boundaries (Cliffe, Jackson & Greenfield 1982; Engleman *et al.* 1982).

The finite-element equations may be written in the form (Cliffe & Spence 1984),

$$\boldsymbol{f}(\boldsymbol{x}, R, \Gamma, \tau) = \boldsymbol{0}, \quad \boldsymbol{f}: \boldsymbol{X} \times \mathbb{R} \times \mathbb{R} \times \mathbb{R} \to \boldsymbol{X} \tag{3.6}$$

where $\boldsymbol{x}$ is a vector containing all the velocity and pressure degrees of freedom. The space $\boldsymbol{X}$ is the set of all possible $\boldsymbol{x}$ and is equivalent to $\mathbb{R}^N$ where N is the total number of degrees of freedom in the problem. The $\boldsymbol{f}$ in (3.6) has an important symmetry property which reflects the fact that the Navier–Stokes equations are invariant under reflection about the mid-plane of the annulus. It can be shown (Cliffe & Spence 1984) that, provided the mesh is symmetric, there exists a linear mapping S from $\boldsymbol{X}$ to $\boldsymbol{X}$ such that

$$S \neq I, \quad S^2 = I \quad \text{and} \quad \boldsymbol{f}(S\boldsymbol{x}, R, \Gamma, \tau) = S\boldsymbol{f}(\boldsymbol{x}, R, \Gamma, \tau), \quad \boldsymbol{x} \in \boldsymbol{X}, \quad R, \Gamma, \tau \in [0, 1]. \tag{3.7}$$

We used the Keller arclength-continuation method to calculate individual solution branches (Keller 1977). The stability limit of the anomalous modes corresponds to either a simple-limit point or a symmetry-breaking bifurcation point. We calculated paths of limit points by applying Keller arclength continuation to the following extended system of equations (Moore & Spence 1980; Jepson & Spence 1984):

$$F(\boldsymbol{y}, \Gamma, 1) \equiv \begin{Bmatrix} \boldsymbol{f}(\boldsymbol{x}, R, \Gamma, 1) \\ \boldsymbol{f}_{\boldsymbol{x}}(\boldsymbol{x}, R, \Gamma, 1)\boldsymbol{\phi} \\ \boldsymbol{l}\boldsymbol{\phi} - 1 \end{Bmatrix} = \boldsymbol{0} \tag{3.8}$$

with $\boldsymbol{y} = (\boldsymbol{x}, \boldsymbol{\phi}, R)$, $\boldsymbol{\phi} \in \boldsymbol{X}$ and $\boldsymbol{l} \in \boldsymbol{X}'$ (the dual of $\boldsymbol{X}$).

The mapping S in (3.7) induces a natural decomposition of $\boldsymbol{X}$ into

$$\boldsymbol{X} = \boldsymbol{X}_{\mathrm{s}} + \boldsymbol{X}_{\mathrm{a}}, \tag{3.9}$$

where

$$\boldsymbol{X}_{\mathrm{s}} = \{\boldsymbol{x} \in \boldsymbol{X} \,|\, S\boldsymbol{x} = \boldsymbol{x}\}, \quad \boldsymbol{X}_{\mathrm{a}} = \{\boldsymbol{x} \in \boldsymbol{X} \,|\, S\boldsymbol{x} = -\boldsymbol{x}\}, \tag{3.10}$$

consist of *symmetric* and *antisymmetric* elements of $\boldsymbol{X}$ respectively. The paths of symmetry-breaking bifurcation points, which occur for the anomalous modes with

an even number of cells, were calculated by applying Keller arclength continuation to the following extended system (Werner & Spence 1984):

$$F(y,\Gamma,1)=\begin{Bmatrix} f(x,R,\Gamma,1) \\ f_x(x,R,\Gamma,1)\phi \\ l\phi-1 \end{Bmatrix}=0, \qquad \begin{aligned} &y=(x,\phi,R)\in Y, \\ &Y=X_s\times X_a\times\mathbb{R}, \\ &F: Y\times\mathbb{R}\times\mathbb{R}\to Y. \end{aligned} \tag{3.11}$$

Note that (3.11) is similar to (3.8) but that the solution x is restricted to be a symmetric vector, whereas the eigenvector ϕ must be antisymmetric.

We now describe the procedure for generating the anomalous modes for the realistic problem with no-slip boundary conditions on the ends of the annulus. To generate an N-cell anomalous mode the first bifurcation in the problem with $\tau=0$ and $\Gamma=N$ was calculated by monitoring the sign of the determinant of the Jacobian matrix, f_x, along the Couette flow branch as the Reynolds number was increased. A change in sign between two values of R indicates the presence of bifurcation. The bifurcating branch, which has N cells, was then followed using the eigenvector at the bifurcation point to construct an initial guess for continuation along the bifurcating branch. In the case of an even number of cells the branch with flow outwards near the ends was chosen; in the odd case either branch will do. The N-cell branch was followed out to a Reynolds number of 300. At this point R and Γ were fixed at 300 and N respectively and Keller continuation was applied to the parameter τ, which was then changed from 0 to 1. The solution with $\tau=1$ and $R=300$, $\Gamma=N$ is then the required anomalous mode for the realistic problem. By this means we found it possible to produce 2-, 3-, 4-, 5-cell anomalous modes.

We should note that the numerical technique used here does not guarantee that the solutions are stable to all types of perturbation. For example, at present, we have no economical means of detecting the presence of a Hopf bifurcation, and no test of stability to non-axisymmetric disturbances has been made.

It is interesting to note that the behaviour of the solution as τ is increased towards 1 is highly nonlinear. In fact the velocities at the ends of the annulus show very little change until τ is greater than about 0.95. This behaviour is another indication that perturbation methods may not be appropriate for this problem.

The region D was covered by a mesh of quadrilateral elements which were uniform in the r- and z-directions except near the corners where the inner cylinder meets the ends, where local refinement was used (see Cliffe 1983, 1984). For calculations of the modes with an even number of cells only half the region D need be discretized (Cliffe & Spence 1984) whereas for modes with an odd number of cells we had to treat the whole of D. The meshes for the full region may be characterized by the triple (NR, NZ, NC) where NR and NZ are the numbers of elements in r- and z-directions respectively and the mesh has $2NC-1$ elements in each corner. A mesh for one half of the region D will be denoted by (NR, NZ, NC, S) and is essentially equivalent to that part of a $(NR, 2NZ, NC)$ mesh with $z\leqslant 0$. The total number of degrees of freedom on a (NR, NZ, NC) mesh is $3(2NR+1)(2NZ+1)+60(NC-1)+3NR, NZ+6(NC-1)$ and on a (NR, NZ, NC, S) mesh is $3(2NR+1)(2NZ+1)+30(NC-1)+3NR, NZ+6(NC-1)$. As in our previous work on the Taylor problem (Cliffe 1983, 1984) we found that the results were insensitive to the value of NC provided it was greater than 4. Most of the calculations were done with NR equal to 10 and NZ equal to NR times the integer nearest Γ. Calculations at a few points were done on finer meshes as a check on accuracy.

4. Experimental procedure

The apparatus used in the experiments is virtually the same as was used by Mullin (1982) and interested readers are referred there for further details. The outer glass cylinder has a precision bore of 63.5 ± 0.04 mm and the inner cylinder is made of machined stainless steel and has a diameter of 38.10 ± 0.02 mm giving a radius ratio of 0.6. The end conditions are symmetric, being provided by two identically machined PTFE collars. It should be noted here that the presence or absence of the bottom collar makes no detectable difference to the results obtained. The photographs were taken with the collar in place to reassure the reader that the observed asymmetric flows are not artefacts of the boundary condition.

The top PTFE collar can be moved vertically in a controlled way by means of a micrometer attachment so that accurate measurements of the aspect ratio can be made and calibrated against an external travelling telescope. The inner cylinder is driven round with a stepping motor system with an accuracy of better than 0.1 % and the temperature of the fluid controlled to within 0.1 °C.

The flow is visualized by adding a small amount of Mearlmaid AA natural pearlessence and illuminated from the side by a slit of light ~ 2 mm wide obtained from a 150 W slide projector outside the temperature control cabinet. The photographs were taken from a position at right angles to the plane of illumination using Kodak Techni-Pan film. The exposure time for each photograph was 8 s at f no. 32 using an 80 mm macro-lens with bellows.

Earlier experiments on anomalous modes by Benjamin & Mullin (1981) were performed using different apparatus. In this case the outer stationary cylinder was made of a selected piece of Perspex tubing. Unfortunately, this appears to have become distorted over a period of time and this may help to explain the quantitative discrepancy between the present results and those obtained previously; the qualitative nature of the results is unaffected by this distortion. The earlier results are consistently 30 % lower in the estimate for critical speeds for collapse of the anomalous modes, except for the single-cell results, which bear good comparison with the numerical work of Cliffe (1983). This may also explain the difference between the numerical and experimental results for the 2–4 cell exchange investigated by Benjamin (1978) and Cliffe (1984). The results there are qualitatively correct but again the experimental points lie below the numerical ones.

The method of generation of the anomalous modes is the same as reported by Benjamin (1978). The apparatus is switched from rest to a final speed in a range above approximately four times that for the first appearance of cells. A range of final speeds is swept out by repeating the process many times and in this way narrow bands are located where anomalous modes can be created repeatedly. Indeed, a pertinent observation is that the anomalous mode is established very rapidly after switch-on with the central cells establishing themselves first and determining the direction of rotation of the end cells. The final speed values used have been found to be different for each apparatus used and are presumably a function of the inertia of the system. However, with practice, any desired anomalous mode may be generated to order over a reasonably large range of aspect ratios.

5. Results

Figure 4 shows the numerically calculated stability curves for the 2-, 3-, 4-cell anomalous modes for radius ratio 0.615, which corresponds to the experiments of Benjamin & Mullin (1981). The solid line indicates a path of limit points and the

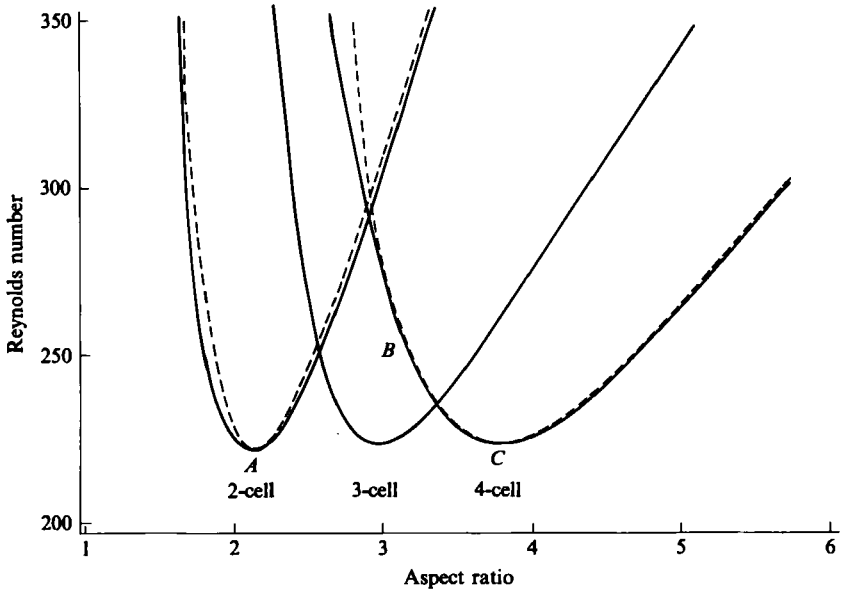

FIGURE 4. Critical loci for 2-, 3- and 4-cell anomalous modes with radius ratio 0.615: ——, numerically calculated fold curve; – – –, numerically calculated path of symmetry-breaking bifurcation points.

dashed line a path of symmetry-breaking bifurcation points (only for the modes with an even number of cells). For aspect ratios lower than that corresponding to A the path of symmetry-breaking bifurcation points lies on the unstable part of the symmetric solution surface whereas it lies on the stable side for aspect ratios greater than A. Thus the 2-cell flow becomes unstable due to antisymmetric disturbances when Γ is greater than 2.2. For the 4-cell modes the path of symmetry-breaking bifurcation points lies on the unstable part of the symmetric solution surface only between B and C. Thus, over most of the range of aspect ratios the 4-cell collapses due to antisymmetric disturbances. Note also that the limit point and symmetry-breaking point appear always to occur at similar values of the Reynolds number as indicated by the closeness of the solid and dotted lines.

The qualitative nature of figure 4 is very similar to that found experimentally by Benjamin & Mullin (1981). However, the critical Reynolds numbers are about 30% higher than those Benjamin & Mullin found. We believe this is due to the imperfections in that apparatus which were discussed in §4. We have not shown the stability curve for the anomalous 5-cell mode since it is more complex than the others. A considerable amount of work will be required to investigate this case properly and it is presently in progress.

Figure 5 shows a comparison of the numerically calculated stability curve and the new experimental data for the 4-cell mode with radius ratio 0.6. Again, in the region between A and B the symmetry-breaking bifurcation points lie on the unstable part of the symmetric solution surface. The experimental points should, therefore, be compared with the dashed curve except between A and B where they should be compared with the solid curve. Tables 1 and 2 indicate mesh refinement tests done at the extremes of this stability curve. From this we conclude that the errors in the numerically calculated curves are less than 1%. The agreement between the theory and experiment is clearly good.

In figures 6, 7 and 8 we give a comparison between the computed streamline plots

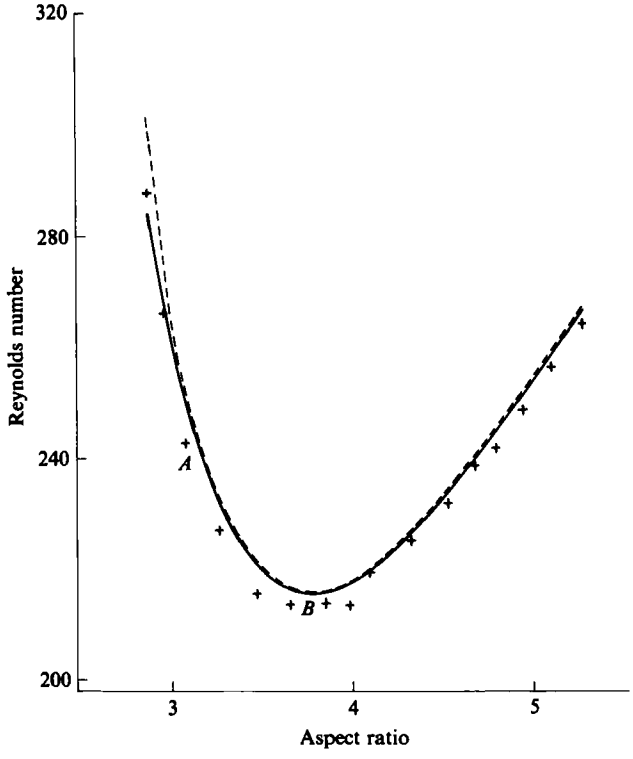

FIGURE 5. Critical loci for the 4-cell anomalous mode with radius ratio 0.6: +, experiment; ——, numerically calculated fold curve; – – –, numerically calculated path of symmetry-breaking bifurcation points.

Mesh	Critical R at aspect ratio 2.87	Critical R at aspect ratio 5.27
10, 20, 5, S	283.85	266.53
15, 30, 5, S	282.48	266.22
20, 40, 5, S	282.20	266.11

TABLE 1. Effect of mesh refinement on the critical Reynolds numbers at the limit points at the two extremes of the fold curve shown in figure 5

Mesh	Critical R at aspect ratio 2.87	Critical R at aspect ratio 5.27
10, 20, 5, S	300.11	267.16
15, 30, 5, S	298.71	266.80
20, 40, 5, S	298.43	266.70

TABLE 2. Effect of mesh refinement on the critical Reynolds numbers at the symmetry-breaking bifurcation points at the two extremes of the path of such points shown in figure 5

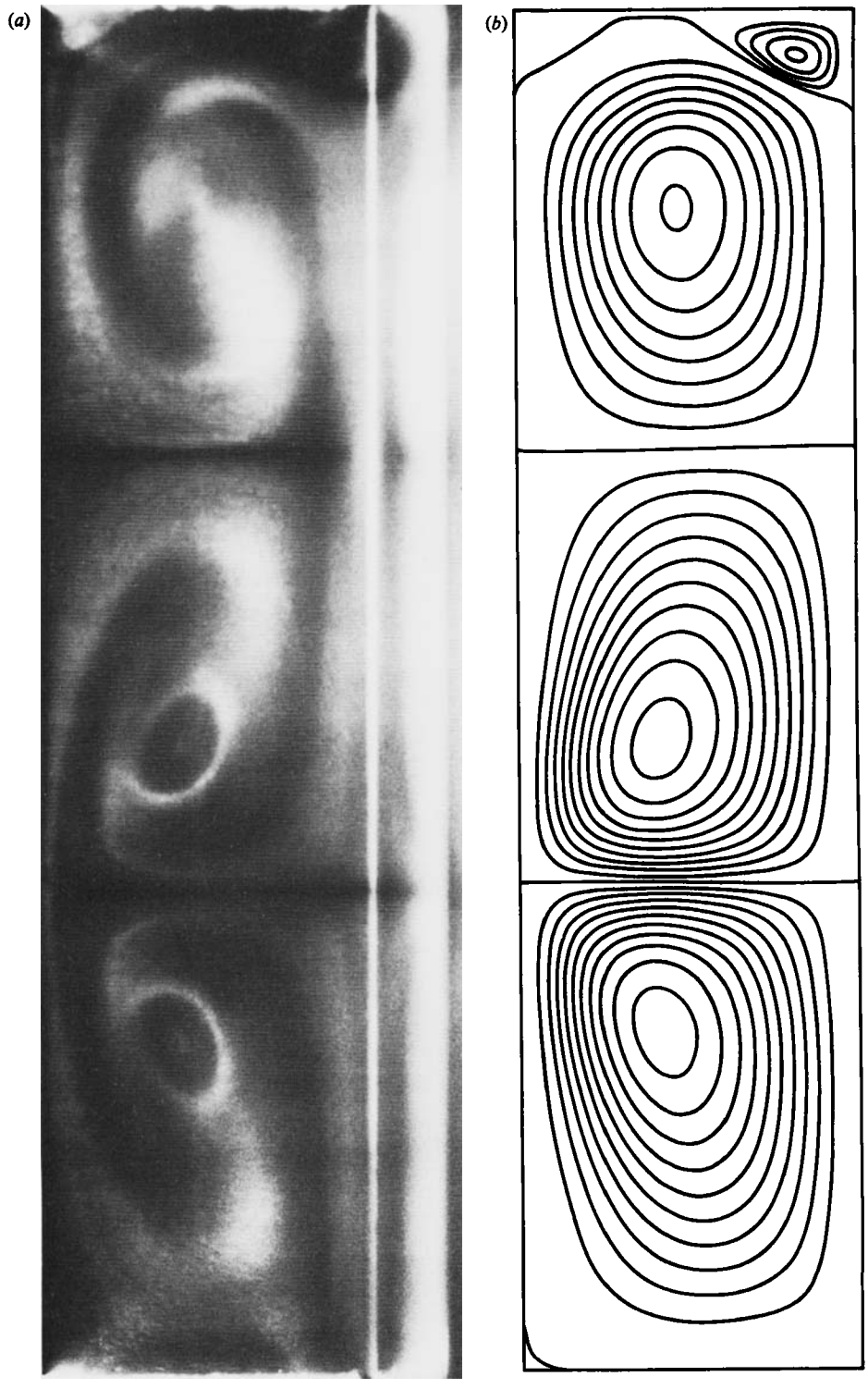

FIGURE 6. Photograph (*a*), and streamline plot of numerical solution (*b*), for $\eta = 0.6$, $\Gamma = 4.0$, $R = 300$ for the 3-cell anomalous mode. Contours of the stream function are plotted at intervals of 0.01 except for the small vortex in the corner where the interval is 0.002. The inner cylinder is at the right hand side.

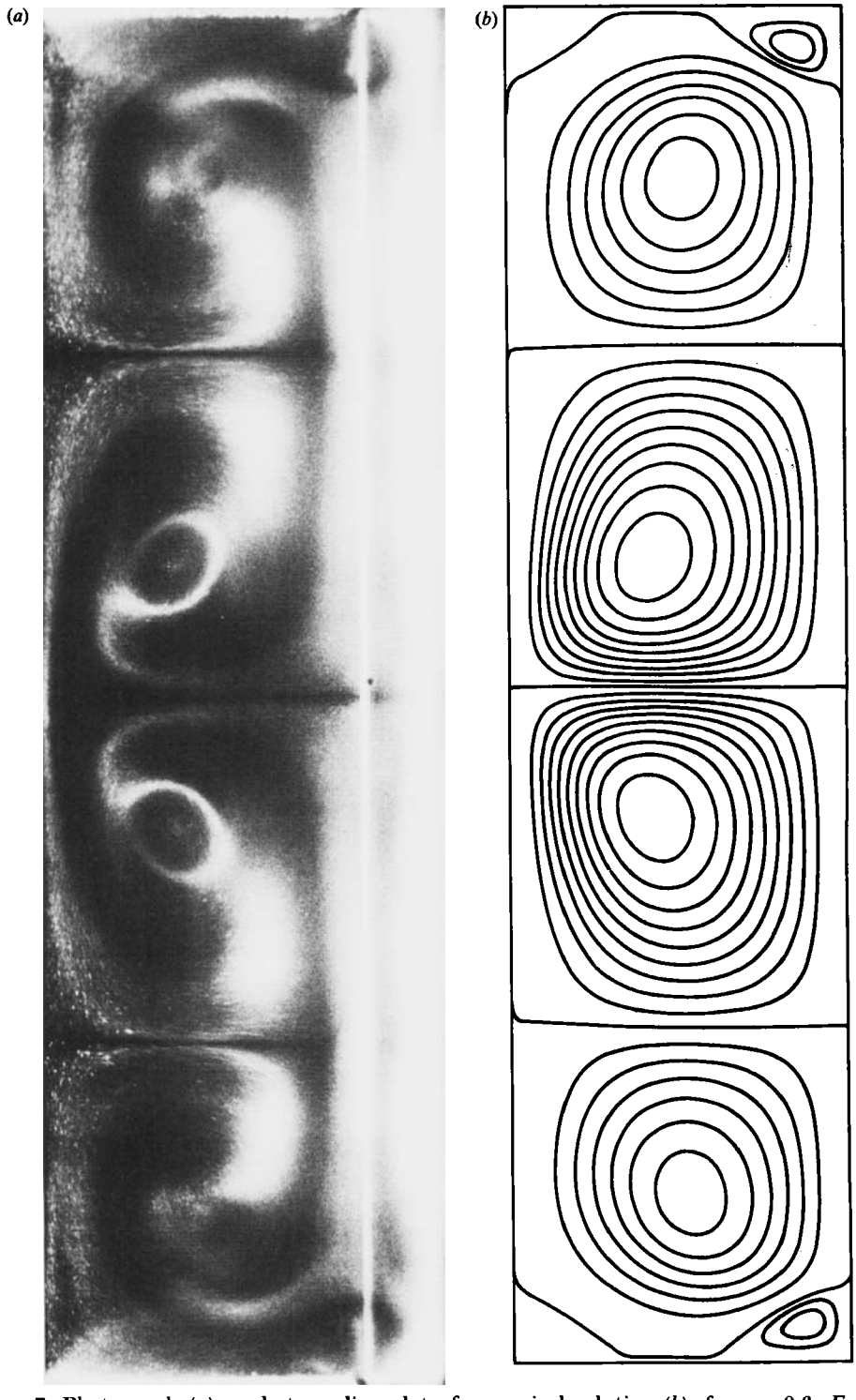

FIGURE 7. Photograph (*a*), and streamline plot of numerical solution (*b*), for $\eta = 0.6$, $\Gamma = 4.0$, $R = 300$ for the 4-cell anomalous mode. Contours of the streamfunction are plotted at intervals of 0.01 except for the small vortex in the corners where the interval is 0.002. The inner cylinder is at the right-hand side.

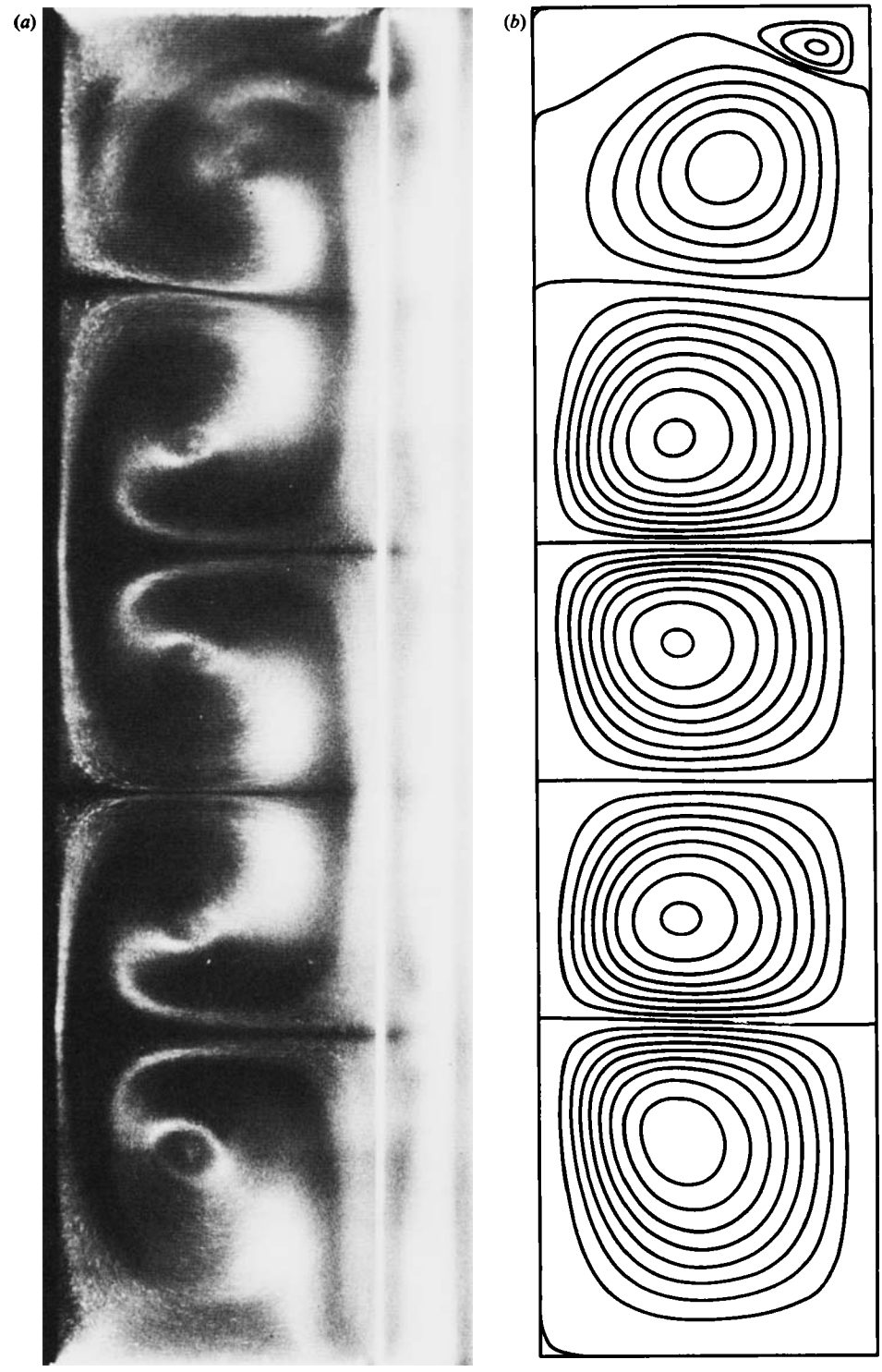

FIGURE 8. Photograph (*a*), and streamline plot of numerical solution (*b*), for $\eta = 0.6$, $\Gamma = 4.0$, $R = 300$ for the 5-cell anomalous mode. Contours of the streamfunction are plotted at intervals of 0.01 except for the small vortex in the corner where the interval is 0.002. The inner cylinder is at the right-hand side.

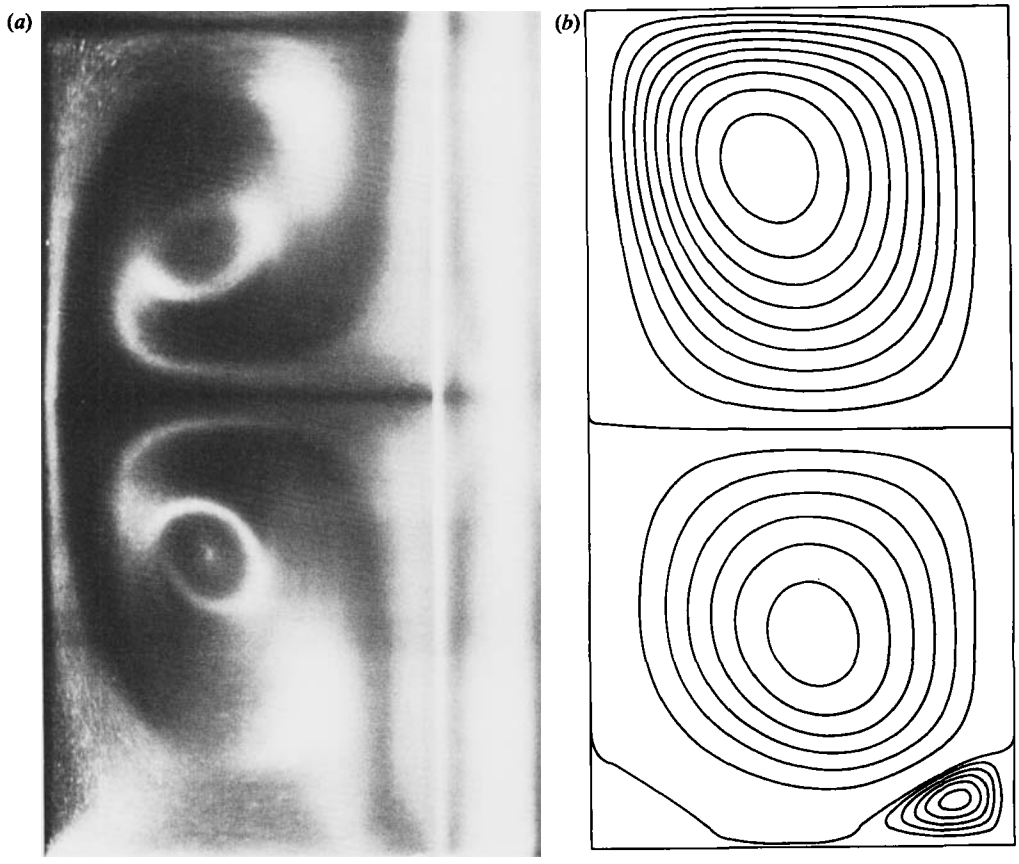

FIGURE 9. Enlarged photograph (*a*), and streamline plot of numerical solution (*b*), for $\eta = 0.6$, $\Gamma = 4.0$, $R = 300$ for the 4-cell anomalous mode showing the small vortex in the corner between the inner, rotating cylinder and the stationary end. Contours of the stream function are plotted at intervals of 0.01 except for the small vortex in the corner where the interval is 0.001. The inner cylinder is at the right-hand side.

and cross-sectional photographs of the 3-, 4-, and 5-cell anomalous modes. The aspect ratio is 4.0 and $R = 300$ for each case. A striking feature of anomalous modes, particularly those with a larger number of cells, is the distortion of the cell boundary adjacent to the anomalous cell. This can be seen clearly in the 5-cell example.

A more obvious feature is the recirculation at the inner corner adjacent to the rotating wall. This feature is shown in enlarged form for the anomalous and normal 4-cell flows in figures 9 and 10. In both cases $R = 300$ and $\Gamma = 4$ and we have displayed only half of the symmetric flows. The striking agreement between these and the other photographs and streamline plots is evident.

6. Conclusions

We have presented new experimental results on anomalous modes in the Taylor experiment and compared them with numerical solutions of the Navier–Stokes equations. The computed streamline patterns show good agreement with photographs of the flows and the numerically determined stability curves for the 4-cell anomalous

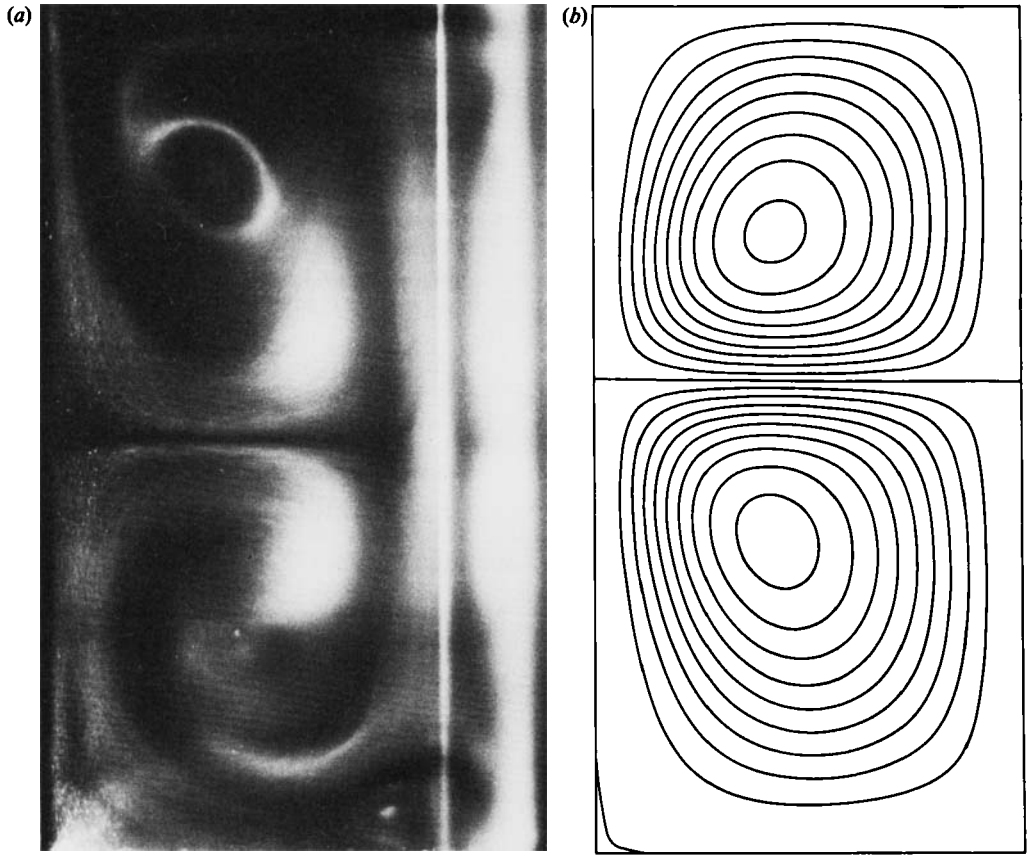

FIGURE 10. Enlarged photograph (*a*), and streamline plot of numerical solution (*b*), for $\eta = 0.6$, $\Gamma = 4.0$, $R = 300$ for the normal 4-cell flow (cf. figure 9). Contours of the streamfunction are plotted at intervals of 0.01. The inner cylinder is at the right-hand side.

mode is in good quantitative agreement with the experimental curve. These results confirm the general conclusions reached by Benjamin (1978) and Benjamin & Mullin (1981) in earlier studies.

We wish to emphasize that, in the light of Schaeffer's (1980) model, the anomalous modes are not at all surprising, indeed they are to be expected. They are due to the ends of the annulus and are an essential feature of the Taylor experiment with realistic end conditions.

We would like to thank Mr C. W. Band of the photographic group of the Physics department at Oxford for his help with the photography and Mr A. C. Greenfield for help with the computing.

REFERENCES

BAUER, L., KELLER, H. B. & REISS, E. L. 1975 Multiple eigenvalues lead to secondary bifurcation. *SIAM Rev.* **17**, 101–122.

BENJAMIN, T. B. 1978 Bifurcation phenomena in steady flows of a viscous liquid. II. Experiments. *Proc. R. Soc. Lond.* A **359**, 27–43.

BENJAMIN, T. B. & MULLIN, T. 1981 Anomalous modes in the Taylor experiment. *Proc. R. Soc. Lond.* A **377**, 221–249.

BENJAMIN, T. B. & MULLIN, T. 1982 Notes on the multiplicity of flows in the Taylor experiment. *J. Fluid Mech.* **121**, 219–230.

CLIFFE, K. A. 1983 Numerical calculations of two-cell and single-cell Taylor flows. *J. Fluid Mech.* **135**, 219–233.

CLIFFE, K. A. 1984 Numerical calculations of the primary flow exchange process in the Taylor problem. Submitted to *J. Fluid Mech.*

CLIFFE, K. A., JACKSON, C. P. & GREENFIELD, A. C. 1982 Finite-element solutions for flow in a symmetric channel with a smooth expansion. *Harwell report* AERE R-10608. HMSO.

CLIFFE, K. A. & SPENCE, A. 1984 The calculation of high order singularities in the finite Taylor problem. In *Numerical Methods for Bifurcation Problems* (ed. T. Küpper, H. D. Mittlemann & H. Weber). Birkhauser: ISNM.

CLIFFE, K. A. & WINTERS, K. H. 1984 A numerical study of the cusp catastrophe for Bénard convection in tilted cavities. *J. Comp. Phys.* **54**, 531–534.

ENGLEMAN, M. S., SANI, R. L., GRESHO, P. M. & BERCOVIER, M. 1982 Consistent vs. reduced integration penalty methods for incompressible media using several old and new elements. *Intl J. Numer. Methods Fluids* **2**, 25–42.

HALL, P. 1980 Centrifugal instabilities in finite containers: a periodic model. *J. Fluid Mech.* **99**, 575–596.

HALL, P. 1982 Centrifugal instabilities of circumferential flows in finite cylinders: the wide gap problem. *Proc. R. Soc. Lond.* A **384**, 359–379.

JEPSON, A. & SPENCE, A. 1984 Folds in solutions of two parameter systems. *SIAM J. Numer. Anal.* (To appear.)

KELLER, H. B. 1977 Numerical solutions of bifurcation and nonlinear eigenvalue problems. In *Applications of Bifurcation Theory* (ed. P. H. Rabinowitz), pp. 359–384. Academic.

LORENZEN, A. & MULLIN, T. 1984 Anomalous modes and finite length effects in Taylor–Couette flow. Submitted to *Phys. Rev.* A.

MOORE, G. & SPENCE, A. 1980 The calculation of turning points of nonlinear equations. *SIAM J. Numer. Anal.* **17**, 567–576.

MULLIN, T. 1982 Mutations of steady cellular flows in the Taylor experiment. *J. Fluid Mech.* **121**, 207–218.

MULLIN, T., CLIFFE, K. A. & BENJAMIN, T. B. 1984 In preparation.

MULLIN, T. & LORENZEN, A. 1984 Bifurcation phenomena between a rotating circular cylinder and a stationary square outer cylinder. Submitted to *J. Fluid Mech.*

SCHAEFFER, D. G. 1980 Analysis of a model in the Taylor problem. *Math. Proc. Camb. Phil. Soc.* **87**, 307–337.

SHEARER, M. 1980 Secondary bifurcation near a double eigenvalue. *SIAM J. Math. Anal.* **11**, 365–389.

WERNER, B. & SPENCE, A. 1984 The computation of symmetry-breaking bifurcation points. *SIAM J. Numer. Anal.* **21**, 388–399.